

The origin of bistability in the butyl-substituted spiro-biphenalenyl-based neutral radical material

Maria Fumanal[†], Juan J. Novoa, Jordi Ribas-Arino*

Departament de Química Física and IQTCUB, Facultat de Química, Universitat de Barcelona, Av. Diagonal 645, 08028-Barcelona (Spain)

* jordi.ribas.jr@gmail.com, j.ribas@ub.edu

[†]*Present address*: Laboratoire de Chimie Quantique, Institut de Chimie UMR7177 CNRS-Université de Strasbourg, 1 Rue Blaise Pascal BP 296/R8, F-67007 Strasbourg, France

Abstract

One of the most remarkable bistable materials so far reported is made of π -dimers of a butyl-substituted spiro-biphenalenyl boron radical (butyl-SBP). The phase transition of this material, which is accompanied by changes in its optical, conductive and magnetic properties, occurs with a hysteretic loop 25-K wide and is centered at 335 K. Here, we present a computational study aimed at deciphering the origin of this hysteresis. We show that the phase transition of butyl-SBP consists of a spin transition of their constituent π -dimers coupled with an order-disorder transition involving the butyl chains linked to the N atoms of the superimposed phenalenyl rings of the π -dimer. Below 335 K, the terminal methyl group of the butyl chains adopts a *gauche* conformation with respect to the methylene unit bonded to the N atom. Above 335 K, the methyl group is in an *anti* conformation and exhibits dynamic disorder. The *gauche* \rightarrow *anti* conformational rearrangement triggers the spin transition of the π -dimers and is responsible for the hysteretic behavior of butyl-SBP. Specifically, the onset of the phase transition in the heating mode and, thus, the width of the hysteresis loop, are governed by the high energy cost and the strong structural cooperative effects associated with this conformational change. Our results show that coupling a spin switch with a conformational switch in a molecular crystal provides a promising strategy in the design of new bistable materials.

Introduction

Bistability is an intriguing phenomenon exhibited by a few materials that present two stable phases that can both exist within a given range of temperatures. Molecule-based bistable materials have been the subject of intense research during the last years because they hold great promise for application in sensors, displays and switching devices.^{1,2,3,4,5} The numerous examples of molecular bistable materials include: materials based on transition metal complexes undergoing spin transitions^{6,7,8,9,10,11,12,13,14}, organic spin-transition materials^{15,16,17,18,19,20,21,22}, compounds whose phase transition is induced by a charge transfer between an electron-donor and an electron-acceptor^{23,24,25,26,27}, compounds featuring charge-transfer-induced spin transitions^{28,29,30}, inorganic-organic hybrid frameworks undergoing phase transitions^{31,32}, molecular crystals whose phase transitions are triggered by changes in the orientation of molecules³³. The transition temperature and the hysteresis loop width of a bistable material are crucial parameters in determining whether its bistability can be harnessed in technological applications. These two parameters, in turn, depend on the intermolecular interactions within the crystal and on the energy barriers associated with the lattice reorganization upon phase transition. For most of the bistable compounds reported so far, very little is known about either the origin of the energy barriers associated with their phase transitions (i.e, whether the energy barrier of the overall phase transition is dominated by a single molecular rearrangement or whether the barrier is the result of the contributions of different reorganization events) nor the role of structural cooperativity in promoting such phase transitions. It is clear that the lack of this sort of information poses a major obstacle for the rational design of new derivatives of a given bistable parent compound with the goal of fine tuning its transition temperature and its hysteresis loop width. Therefore, the studies aimed at elucidating the origin of these barriers and at establishing the role of cooperative effects have the potential to offer most valuable hints on how to devise new bistable materials with improved properties. Here, on the basis of a computational study, we disclose the origin of the hysteretic phase transition of a phenalenyl-based butyl-substituted neutral radical, which is one of the most prominent compounds within the family of bistable materials.

Phenalenyl (PLY) is an odd-alternant hydrocarbon neutral radical arising from a triangular fusion of three benzene rings. This open-shell molecule has emerged in the past years as one of the most versatile building blocks for functional molecular devices

and materials.^{16,34,35,36,37,38,39,40} The numerous spiro-biphenalenyl (SBP) boron radicals reported by Haddon and coworkers constitute a very important class of PLY derivatives.^{41,42,43,44,45,46,47,48,49,50,51,52,53,54,55,56,57} SBPs present two nearly perpendicular phenalenyl units connected through a boron spiro-linkage. The N- and O-functionalized SBPs (*ie*, SBPs in which each phenalenyl unit is bonded to the central boron atom via an oxygen and a nitrogen atom) exhibit diverse packing motifs in the solid state, and hence different physical properties, depending on the substituents attached to the nitrogen atom. Ethyl (**1**) and butyl-substituted (**2**) SBPs (see Figure 1) present a crystal structure containing π -dimers as the basic building block (see Figure 2 and Figure S1). These two compounds undergo a phase transition that is accompanied by a change in their optical, conductive and magnetic properties.^{16,42} The phase transition of ethyl-SBP is reversible and occurs at about 140 K, while that of butyl-SBP occurs with an hysteretic loop 25-K wide and is centered at a much higher temperature (\sim 335 K). At this point, it is worth mentioning that butyl-SBP is one of the few multifunctional bistable materials that switch the response in multiple physical channels upon phase transition.^{25,30,32,26} Besides, the volume of the crystals of butyl-SBP significantly change upon phase transition; specifically, a notable expansion of the crystal is observed when the system switches from its low-temperature (LT) phase to its high-temperature (HT) phase.⁵⁸ This volume change in response to external stimuli is currently a sought-after phenomenon in the context of new functional materials due to its potential applicability to microscale or nanoscale actuators.³³

The experimental^{58,59} and theoretical studies^{60,61,62,63,64} conducted over the last years on ethyl- and butyl-SBP have culminated in a clear understanding of their electronic structure and the different magnetic and conducting properties of their phases. Upon phase transition in the heating mode, the constituent π -dimers of these materials undergo a spin transition from a closed-shell diamagnetic singlet state to an open-shell paramagnetic state. Below the spin transition temperature, the structures of the π -dimers are governed by the potential energy surface (PES) of the ground singlet state (1A_g state), whose minimum structure features a partial localization of the unpaired electrons of each SBP radical in the superimposed phenalenyl (sup-PLY) rings, that is, on the phenalenyl (PLY) units directly involved in the π -dimer (see Figure 2a). The strong coupling between the SBP unpaired electrons in this configuration leads to a magnetically silent state, and, thus, to a diamagnetic LT phase. Above the spin transition temperature, the π -dimers adopt a configuration characterized by a localization of the SBP unpaired electrons in the nonsuperimposed phenalenyl (non-PLY) units, that is, on the PLYs not directly involved in the π -dimer (see Figure 2b),

which leads to a paramagnetic phase. This configuration is exclusively governed by the PES of the ground triplet state (3A_u state) because the corresponding open-shell singlet does not feature any minimum in that region of the PES even if it lies slightly below in energy than the triplet state. In a recent article⁶⁴, we have shown that the high-spin (HS) state is energetically competitive with the low-spin (LS) state because the electrostatic component of the interaction energy between SBP radicals in the π -dimers is more attractive in the high-temperature 3A_u state than in the low-temperature 1A_g state. This electrostatic stabilization of the high-temperature 3A_u state was ascribed to the zwitterionic nature of the SBP moieties, in particular, to the interaction between the positively-charged superimposed PLYs in the triplet state (Figure 2b) and the negatively-charged spiro-linkages with the central boron atom. These electrostatic interactions also explain why the unpaired electrons prefer to localize on the nonsuperimposed PLYs in the high-temperature triplet state.⁶⁴

Despite the current good understanding of the electronic structure of the π -dimers of ethyl- and butyl-SBP and several theoretical studies on other phenalenyl-based systems^{65,66,67,68,69,70,71,72,73,74,75,76,77,78}, there are two crucial questions concerning the phase transitions of ethyl- and butyl-SBP that remain unsettled, namely: i) why is the transition temperature of butyl-SBP so much higher than that of ethyl-SBP?, and ii) why does butyl-SBP display an hysteretic phase transition, in contrast with ethyl-SBP, which features a smooth phase transition? A meticulous study carried out by Haddon and coworkers in Ref. 58 on numerous crystal structures of butyl-SBP at different temperatures led to the suggestion that the HT phase is the thermodynamically stable phase within the bistability region, while the existence of the LT phase within the hysteretic loop was rationalized on the basis of the large energy barrier that the system needs to overcome when switching from LT to HT. Even if this barrier was estimated to be larger than 24 kcal/mol, the specific molecular rearrangements responsible for that barrier were not identified. In the computational study herein presented, not only do we provide a rationale for the higher spin-transition temperature of butyl-SBP but also disclose the hitherto elusive origin of its hysteresis loop. In particular, our study reveals that the bistability arises from a very simple molecular rearrangement, namely, a conformational rearrangement of the butyl groups attached to the SBP radicals.

Results and discussion

The presentation of the results is organized as follows. We will first demonstrate that the higher phase-transition temperature of compound **2** (compared to that of **1**) arises from a coupling of its spin transition with a conformational rearrangement of the butyl groups (*subsection 1*). Then, we will disclose that the significant expansion of crystals of **2** upon LT→HT phase transition is governed by this very conformational rearrangement of butyl groups (*subsection 2*). After that, we will show that the dynamic disorder exhibited by the butyl chains in the high-temperature phase of **2** implies that the conformational change of these chains brings about an order-disorder transition (*subsection 3*). Finally, we will decipher the mechanism of the coupling between the spin transition and the conformational rearrangement, we will demonstrate that the LT→HT phase transition is assisted by structural cooperative effects, and we will reveal that the hysteresis loop featured by **2** originates in the high-energy penalty associated with the conformational change of the butyl groups in the crystal lattice of the low-temperature phase (*subsection 4*).

1) Phase transition of butyl-SBP: a spin transition coupled with a conformational rearrangement of the butyl groups.

As mentioned in the Introduction, the phase transition undergone by **1** and **2** is a spin transition in which the corresponding SBP π -dimers switch between two states: a singlet state (1A_g) and a triplet state (3A_u). The low-spin (LS) state is the thermodynamically stable state at low temperatures (LT), while the high-spin (HS) state is the thermodynamically stable state at high temperatures (HT). In the LS state the unpaired electrons of the SBP are strongly coupled and mainly localized in the superimposed PLY units (see HOMO in Figure S2a), while in the HS state they move to the non-superimposed PLYs (see one of the two SOMO in Figure S2b).

In this subsection, we shall first investigate why the spin-transition of **2** is shifted 200 K towards higher temperatures with respect to the spin-transition temperature of **1**. The key quantity to rationalize this behavior is the adiabatic energy gap between the LS and HS minima ($\Delta E^{\text{adia}} = E_{\text{LS}} - E_{\text{HS}}$). The values of ΔE^{adia} in the gas phase and in the solid state for **1** and **2** were evaluated upon geometry optimization of the corresponding isolated π -dimers and the π -dimers in the crystalline phases. The initial configurations for these geometry optimizations were taken from the LT and HT X-Ray nuclear

coordinates (Table S1 and Table 1, respectively). As previously reported⁶⁴, the ΔE^{adia} obtained for compound **1** in the solid state is -2.6 kcal/mol. This value is virtually identical to that found in the gas phase, which means that ΔE^{adia} is not affected by the crystal packing. On the other hand, the ΔE^{adia} values for an isolated π -dimer and for a π -dimer in the solid-state of compound **2** are -3.6 and -9.5 kcal/mol, respectively. The larger adiabatic gap in the solid state for **2** (compared to that of **1**) is in line with its higher spin-transition temperature. The large difference between the solid-state and gas-phase ΔE^{adia} values of **2**, in turn, reflects the notable influence exerted by crystal-packing effects on the spin-transition properties of this material. It is worth mentioning that such effects have already been observed in Fe(II)-based spin crossover compounds.^{79,80,81} In the following, we shall examine the origin of the different ΔE^{adia} values of ethyl and butyl-SBP.

A close inspection of the X-ray crystal structures of **1** and **2** brings to light a notable difference in the conformational behavior of their alkyl chains. While the conformation of the ethyl group of **1** is the same below and above the phase transition temperature, the butyl group of **2** changes its conformation upon phase transition. Specifically, in the LT structures of **2**, the terminal methyl groups of the butyl chains attached to the N atoms of the superimposed PLYs are in a *gauche* arrangement with respect to the methylene groups linked to the N atoms (see Figure 2a). Conversely, in the HT structures of **2**, the terminal methyl groups of the butyl chains attached to the N atoms of the superimposed PLYs are in *anti* with respect to the methylene groups linked to the N atoms (see Figure 2b). The different conformations adopted by the butyl chains of **2** in its LT and HT phases raise the question of which is the role of the conformational flexibility of the butyl chains in the phase transition of this compound. We shall now turn our attention to this issue. Note that the butyl chains linked to the N atoms of the non-PLY rings do not change their conformation in going from LT to HT. Hence, in what follows we will not deal with the conformations of these particular butyl chains.

So far, we have shown that the LS state of the π -dimers of **2** in combination with the *gauche* conformation of the butyl chains give rise to a minimum energy configuration that will hereafter be referred to as LS(*gau*) configuration. We have also shown that the combination of the HS state of the π -dimers and the *anti* conformation of the butyl chains gives rise to another minimum energy configuration, which will be referred to as HS(*anti*) configuration. We only considered these two configurations since they correspond to the experimental observation. However, at this point, one could

hypothesize that the LS(*anti*) and the HS(*gau*) configurations might also exist as minima even if they have not been experimentally detected. Variable-cell optimizations demonstrated that the LS(*anti*) and HS(*gau*) configurations correspond indeed to minima. A scheme of the relative energies of the different polymorphs of **2** considered in this work is presented in Figure 3. The most stable polymorph of **2** is the LS(*gau*) polymorph, in agreement with the fact that this is the phase detected at low temperatures for compound **2**. Concerning the polymorphs containing π -dimers in their HS state, our calculations bring to light that HS(*gau*) is lower in energy than HS(*anti*), even if the polymorph experimentally detected at high temperatures is the latter one. The energetic preference for the *gauche* conformations in the condensed phase (irrespective of the spin state of the π -dimers) is also observed for isolated π -dimers (see Figure 3)⁸².

The different ΔE^{adia} values reported in Figure 3 shed light on the origin of the different spin transition temperatures of compounds **1** and **2**. Interestingly, the ΔE^{adia} value between the polymorphs featuring *anti* conformations of their butyl chains is equal to the ΔE^{adia} value of compound **1**⁸³. This proves that the large difference between the LS(*gau*)-HS(*anti*) adiabatic gap in compound **2** (-9.5 kcal/mol) and the adiabatic gap of compound **1** (-2.6 kcal/mol) is due to the conformational rearrangement of the butyl chains in the former compound upon phase transition. The large values of the LS(*gau*)-LS(*anti*) and HS(*gau*)-HS(*anti*) gaps provide further evidence that the conformational changes of the butyl chains bring about important modifications of the intermolecular interactions in the condensed phase, which lead to a notable destabilization of the *anti* polymorphs. It is thus concluded that the higher phase-transition temperature of **2** (compared to that of **1**) stems from the coupling between an electronic transition and a conformational change.

2) Origin of the main structural differences between the two polymorphs of **2**.

The detailed structural analysis reported by Haddon and coworkers in Ref.58 showed that the main structural differences between the LT and HT polymorphs of **2** are the interplanar distance between the sup-PLY units of the π -dimers (*D*) and the distance associated with a CH $\cdots\pi$ interaction formed by an aromatic C-H of one π -dimer and one of the sup-PLY rings of a neighboring π -dimer (see Figure S3 for definition). Both types of distances increase by 0.1 Å upon LT \rightarrow HT phase transition. Furthermore, this

phase transition is accompanied by a large change in the unit cell volume, which increases by 3.5% in going from LT to HT. As shown in Table 2, all these structural changes detected in the X-ray crystals are properly captured by the optimized structures of the LS(*gau*) and HS(*anti*) polymorphs. We shall now trace the origin of these structural changes.

The results collected in Table 2 show that for a given conformation of the butyl groups (be it either *gauche* or *anti*) the D value (see Figure S3 for its definition) of the π -dimers in the optimized HS polymorphs is *ca.* 0.08 Å larger than in the optimized LS polymorphs. On the other hand, for a given spin state of the π -dimers (be it either LS or HS), the D value in the optimized *anti* polymorphs is *ca.* 0.05 Å larger than in the optimized *gauche* polymorphs. It then follows that the increase of D upon LT→HT phase transition is due to both the change in the spin state of the π -dimers and the conformational rearrangement of the butyl chains, the former effect being the dominant one. On the contrary, the increase of the CH $\cdots\pi$ distance upon LT→HT phase transition should be mainly ascribed to the conformational rearrangement of the butyl groups (see Table 2).

Finally, the results of Table 2 show that a LS→HS spin transition by itself (*ie*, a spin transition that is not accompanied by any conformational change of the butyl chains) entails only a very small volume cell increase (*ca.* 0.4%), similarly to that reported for compound **1**. In stark contrast, Table 2 discloses that for a given spin state (be it either LS or HS) the *gauche*→*anti* conformational rearrangement of the butyl chains brings about an increase of *ca.* 4% in the volume unit cell. It is thus concluded that the remarkable volume increase of compound **2** upon LT→HT phase transition originates in the conformational change of its butyl chains. As shown in Table S2, the experimentally observed increase in the volume unit cell mainly originates in the increase of the cell parameter b , which lengthens by about 0.3 Å upon LT→HT phase transition. The notable elongation of b can be understood on the basis of the fact that the butyl chains lie parallel to this axis when they adopt the *anti* conformation.

3) Driving forces of the phase transition of butyl-SBP. Order-disorder transition involving the butyl chains.

We shall now focus on the driving force of the complex phase transition undergone by **2**. In our previous study of compound **1**⁶⁴, we demonstrated that the HS state of the π -dimers have a larger vibrational and electronic entropy than the LS state, as a result of which the HS state become the thermodynamically stable state above a certain temperature. As observed in Figure 4 (red curve), the HS(*gau*) state of an isolated π -dimer of **2** is also entropically stabilized with respect to the LS(*gau*) state. The key question at this point is whether the *gauche* \rightarrow *anti* conformational change is accompanied by any extra change in the vibrational entropy of the system. The green curve of Figure 4 proves that this is indeed the case for isolated π -dimers. Such trend is not only maintained but also enhanced in the solid state (dashed green line of Figure 4). As a result of the extra gain in vibrational entropy in going from a *gauche* to an *anti* conformation, the entropic stabilization of the HS(*anti*) configuration of the π -dimers of **2** with respect to the LS(*gau*) configuration as the temperature increases is much larger than the entropic stabilization of the HS state with respect to the LS state in compound **1** (see dark blue curve in Figure 4). The large vibrational entropy gained by the π -dimers of **2** when their butyl chains adopt an *anti* conformation is thus crucial in enabling this compound to clear a HS(*anti*)-LS(*gau*) adiabatic gap that is much larger than the HS-LS adiabatic gap of compound **1**.

The fact that the hysteretic phase transition of butyl-SBP is centered at a high temperature (~ 335 K), together with the large thermal ellipsoids of the carbon atoms of the butyl chains observed in the X-ray crystal structure of the HT phase of **2**⁵⁸, strongly suggest that going beyond the static perspective so-far adopted in this article by explicitly considering the thermal fluctuations of the system might offer an improved description of the phase transition of butyl-SBP. The thermal fluctuations of the system were considered by performing *ab initio* molecular dynamics simulations (AIMD) for the LT and HT phases of compound **2**. These AIMD simulations, which span a time interval of more than 60 picoseconds, were done at 340 K because this temperature is within the hysteresis loop. The simulation box of the unit cell employed in the simulations includes four spiro-biphenalenyls monomers, which gives rise to two π -dimers, such that the dynamics of four non-equivalent butyl-ligands bonded to the sup-PLY was followed along the trajectories (see Figure S3). The conformational dynamics of the butyl chains can be analyzed by monitoring the time-resolved evolution of the dihedral angle (θ) between the carbon atom bonded to the N atom and the carbon atom of the terminal methyl group along the central C-C bond of the butyl chain (see Figure 5 for the definition of θ). For practical purposes, the *anti* conformer will hereafter be considered as the reference conformation, which means that the *anti* conformation will

be associated with a dihedral angle of $\theta=0$ and the rest of θ values will be given with respect to the position of the terminal methyl group in the *anti* conformation (Figure 5).

The AIMD simulations of LT-340 (Figure 6a) show that the butyl groups present most of the time a conformation for which $\theta \approx -107^\circ$. As shown in Figure 5, this value of θ corresponds to a *gauche* conformation in which the terminal methyl group is pointing to a non-PLY unit (*gauche*-IN conformation). Sporadic transitions to another conformation for which $\theta \approx 107^\circ$ took place individually on three of the four butyl-groups. In this conformation, the butyl chain is in another *gauche* conformation in which the terminal methyl group is not pointing to a non-PLY (*gauche*-OUT conformation, see Figure 5). The simulations also show that the probability of a given butyl chain to be in the *anti* conformation is of ca. 4%, thus suggesting that this spatial arrangement is energetically disfavored in the unit cell of the LT phase at 340 K.

Two simulations were performed for the HT-340 structure. One simulation was computed starting from the *anti* polymorph, whereas the second one was performed by initially defining a *gauche*-IN position for all butyl-ligands bonded to the sup-PLY units. This strategy allows us to ensure that the conformational sampling is independent from the starting configuration defined. The trajectory of the HT-340 structure that evolves from an initial *anti* conformation shows that, after 15-20 ps, two of the butyl-groups abruptly change their positions adopting a *gauche*-IN conformation whereas the other two go to *gauche*-OUT positions (Figure 6b). Thereafter, eventual transitions between the three possible conformations are detected. On the other hand, the trajectory that starts from the *gauche*-IN polymorph shows that, as in the previous simulation, the four butyl-groups adopt the three possible conformations at some point during the dynamics (Figure 6c). Therefore, our simulations demonstrate that the butyl chains of the HT phase feature a dynamic disorder between three different conformations: *gauche*-IN, *anti* and *gauche*-OUT. This dynamic disorder is in line with the elongated thermal ellipsoids observed for the carbon atoms of the butyl chains in the crystal structures of HT for compound **2**⁵⁸. In contrast, the LT phase of **2** does not exhibit conformational disorder. The appearance of a small amount of disorder in the latter phase during our simulations is ascribed to the proximity to the transition temperature. In light of this analysis, the LS(*gau*) \rightarrow HS(*anti*) phase transition undergone by **2** should be described as a *spin transition coupled with an order-disorder transition*. In the next subsection we shall rationalize the different dynamics featured by the butyl chains in the LS(*gau*) and the HS(*anti*) polymorphs of **2**.

The dynamic disorder found for the butyl chains in the HT phase of **2** strongly suggests that the vibrational entropy of HT is largely underestimated when using the harmonic approximation, as done to obtain the results displayed in Figure 4. It thus follows that the $T\Delta S_T$ values of the blue and both the green curves of Figure 4 would be larger (in absolute value) if the anharmonic effects associated with the dynamic disorder had been taken into account in the calculations. The extra entropic stabilization of the HS(*anti*) polymorph by virtue of the dynamic disorder of its chains supports the mechanism proposed by Haddon and coworkers⁵⁸, which ascribes the presence of the LT polymorph within the hysteresis loop due to the existence of an energy barrier to reach the HT phase, which is the thermodynamic free energy minimum in the range of temperatures of the bistability mainly due to its large vibrational entropy term. The key question that needs to be addressed at this point (see next subsection) is which is the origin of the barrier that LT needs to overcome to transform into the HT phase.

4) Origin of the hysteresis and the coupling between the spin transition and the conformational change in the phase transition of butyl-SBP

In this subsection we shall first rationalize the different dynamics exhibited by the butyl chains of **2** in its LT and HT polymorphs at 340 K. This analysis will also reveal the origin of the energy barrier responsible for the hysteretic phase transition in butyl-SBP. In the last part of this subsection, we shall disclose the origin of the coupling between the spin transition and the conformational rearrangement of the butyl chains in the phase transition of **2**.

The dynamic behavior of the butyl chains can be understood on the basis of the potential energy profile of a butyl chain along the θ dihedral angle. The energy profiles were evaluated by means of a set of constrained optimizations in the solid state in which the θ dihedral angle of one butyl chain of the unit cell was kept fixed at different values while allowing the rest of coordinates to relax. We first computed two energy profiles: one of them using the cell parameters associated with the LT-340 crystal structure and the other one using the cell parameters of the HT-340 crystal structure. Since the separation between adjacent radicals along the cell vector b increases in going from LT-340 to HT-340, the use of these two unit cells enables the investigation of how the conformational landscape of the butyl groups changes upon expansion of the crystal.

As displayed in Figure 7, the most stable conformation of the butyl chain in LT-340 is the *gauche*-IN ($\theta = -107^\circ$) conformation. This explains why this is the most sampled conformer during the AIMD simulations (Figure 6a). The *anti* conformation ($\theta = 0^\circ$) in turn features a shallow minimum that lies *ca.* 4 kcal/mol above the *gauche*-IN conformer. For this reason, this particular conformation is seldom sampled during the AIMD simulations (Figure 6a). The significant increase of the cell vector *b* in going from LT-340 to HT-340 brings about a change in the energetic ordering of the conformers. As shown in Figure 7, the *anti* conformer is the most stable conformation in HT-340, while the *gauche*-IN conformer lies only ~ 2 kcal/mol above. The flatter conformational landscape of HT-340 (as compared with that of LT-340) provides a rationale for the dynamic disorder of the butyl chains observed in the AIMD simulations of HT-340.

The red profile of Figure 7 reveals that there exists a significant energy barrier of *ca.* 5 kcal/mol for the conversion of the *gauche*-IN conformer of a butyl chain into its *anti* conformer in the LT-340 crystal. This result led us to hypothesize that this activated conformational rearrangement is the origin of the energy barrier associated with the LT \rightarrow HT phase transition of compound **2**, and, thus, the origin of its bistability. At first glance, a barrier of ~ 5 kcal/mol would seem too small for a phase transition that occurs at a temperature as high as ~ 350 K in the heating mode. However, the green profile of Figure 7 demonstrates that this barrier markedly increases upon lowering the temperature. Specifically, this barrier goes up to ~ 12 kcal/mol when the conformational rearrangement of a butyl group takes place in the LT-0 crystal (*i.e.*, in the optimized LT polymorph at 0 K). Such an increase of the barrier upon lowering the temperature originates in the thermal contraction of the crystal.

The X-ray resolved structures of the LT phase at 100 and 340 K (see Table S3) show that the shrinkage of the vector cell *c* is one of the main structural changes undergone by the LT phase upon cooling. This is in line with our computational results, which show that the computed vector cell *c* at 0 K is significantly smaller than that of the crystal structures refined at finite temperatures (Table S3). Concomitantly with this variation, some key intermolecular distances also decrease upon cooling. As shown in Figure 8, the thermal contraction of the crystal in the *c* direction results in a shorter H \cdots H contact between one hydrogen atom of the terminal methyl group of a butyl chain and one hydrogen atom of a PLY ring of the adjacent SBP radical (the H \cdots H distance decreases 0.25 Å upon cooling). This H \cdots H contact thus exerts a notable influence on the profiles of Figure 7 and, more specifically, plays a crucial role in modulating the energy barrier that separates the *gauche*-IN and *anti* conformations. At lower

temperatures, the shorter intermolecular contacts give rise to a large steric hindrance, which results in a large energy barrier for the conformational rearrangement. Therefore, the butyl chains cannot undergo the *gauche*-IN \rightarrow *anti* conformational change until the LT phase of **2** reaches a sufficiently high temperature such that the accompanying thermal expansion of the crystal leads to a sufficiently small energy barrier that can be surmounted. It is thus concluded that the barrier associated with this very conformational rearrangement is responsible for the hysteretic phase transition of **2**.

Having reached this point, it should be stressed that the energy barrier discussed in the two previous paragraphs corresponds to the conformational switch of a single butyl chain. The phase transition of **2** entails many of these conformational switches and each of them is an activated process. Therefore, this phase transition cannot be rationalized by means of a single energy barrier. The key question at this point is whether the phase transition is assisted by cooperativity, that is to say, whether the conformational switch of a given butyl chain favors the conformational switch of the butyl chain of a neighboring SBP radical. In order to explore the role of cooperativity, the LS(*gau*) \rightarrow LS(*anti*) phase transition was driven by successively rotating the butyl chains of our simulation cell from a *gauche*-IN to an *anti* conformation (overall, we manually induced four conformational rearrangements). After every rotation to an *anti* conformation, the system was allowed to relax by means of a variable-cell optimization and the change in energy of the system due to the conformational switch was then evaluated. As shown in Figure 9, the first conformational switch of a butyl chain entails a large energy penalty of 10.6 kcal/mol (the energy barrier associated with this process is 12 kcal/mol; see Table S4). Among the three different existing possibilities for the rotation of a second butyl group, the one requiring a smaller energy cost is the conformational switch of the butyl group belonging to the same π -dimer of the butyl group that underwent the first switch. Should the conformational rearrangements of the butyl chains occur independently from each other, the rotation of the second butyl chain would entail an energy penalty of 10.6 kcal/mol. In stark contrast with this scenario, our calculations reveal that the rotation of the second butyl chain entails an extra energy penalty as small as 1.8 kcal/mol (Figure 9). The conformational switch of a third butyl chain, in turn, has an associated extra cost of 4.1 kcal/mol (Figure 9). Finally, the rotation of the fourth butyl group causes a stabilization of the system (Figure 9). It is thus concluded that cooperativity plays a key role in driving the phase transition of **2**. The strong cooperative effects in the LS(*gau*) \rightarrow LS(*anti*) phase transition have also been evaluated by means of the calculation of intermolecular

couplings⁸⁴ and by means of the Slichter-Drickamer model⁸⁵, as was previously done to assess the cooperativity and the hysteretic phase transitions of Fe(II)-based spin-crossover materials^{86,87} (see Supporting Note 1 for a detailed explanation).

We shall now focus on the origin of the coupling between the spin transition and the conformational rearrangement in the phase transition of **2**. The existence of this coupling means that one of these switches (either the spin switch or the conformational switch) triggers the other one. Should the two switches take place independently of each other, either the HS(*gau*) or LS(*anti*) polymorphs would have been detected as intermediate phases in the phase transition of **2**. Therefore, elucidating the origin of this coupling amounts to addressing the following question: why does the LT → HT phase transition bring the system from LS(*gau*) directly to HS(*anti*) without either HS(*gau*) or LS(*anti*) being detected as intermediate phases? Obviously, this question is analogous to the following one: why does the HT → LT phase transition drive the system from HS(*anti*) directly to LS(*gau*) without either HS(*gau*) or LS(*anti*) being detected as intermediate phases? As explained in detail below, the different energy gap between the HS and LS states of the π -dimers of **2** in the solid state depending on the conformation of the butyl chains is key to understand why neither the HS(*gau*) nor the LS(*anti*) polymorphs are observed. While the energy gap between the HS and LS states when the butyl chains adopt an *anti* conformation is 2.6 kcal/mol, this gap increases up to 3.7 kcal/mol when the butyl chains adopt a *gauche*-IN conformation (Figure 3). For our purposes, it is important to remember that the gap of 2.6 kcal/mol coincides with the HS-LS gap found for compound **1**⁶⁴, whose phase transition takes place at ~140 K.¹⁶

Let us now consider the mechanism of the HT→LT phase transition of **2**. Starting from the HS(*anti*) polymorph, there are two conceivable mechanisms for the phase transition in the cooling mode: i) HS(*anti*) → LS(*anti*) → LS(*gau*), or ii) HS(*anti*) → HS(*gau*) → LS(*gau*). Note that the first mechanism entails a spin switch as a first step, followed by a conformational switch. The second mechanism, in turn, entails a conformational switch as a first step, followed by a spin switch. Should the phase transition of **2** occur *via* the first mechanism, such phase transition would have been observed at temperatures around 140 K because the energy gap between HS(*anti*) and LS(*anti*) coincides with the HS-LS gap for compound **1**. Yet the phase transition in the cooling mode of **2** occurs at much higher temperatures (~320 K), i.e, in a temperature range in which HS(*anti*) should still be more stable (in terms of free energy) than LS(*anti*). This means that we can safely rule out the first mechanism. It is thus concluded that the first

step in the phase transition of **2** in the cooling mode is the HS(*anti*) \rightarrow HS(*gau*) transformation. Having established which is the first step in the phase transition of **2** upon cooling, we shall now explain why the conformational switch induces the spin switch of the π -dimers of **2**. As mentioned above, the conformation adopted by the butyl chains exerts a notable influence on the HS-LS energy gap of these π -dimers. When switching from the *anti* to the *gauche* conformation of the butyl chains, the HS-LS energy gap increases by 1.1 kcal/mol. As a consequence of the larger HS-LS gap, the LS state is the thermodynamically stable state over a wider range of temperatures that extends much beyond 140 K. In particular, as inferred from the red curve of Figure 4, which accounts for the entropy that is needed to clear the energy gap upon phase transition, an increase of 1.1 kcal/mol in the energy gap leads to a large broadening of about 200 K of the temperature range in which the LS state is the thermodynamically stable state. As a result of this, at the phase transition temperature in the cooling mode (\sim 320 K), the LS state is more stable than the HS state and, consequently, once the π -dimers find themselves in the HS(*gau*) configuration after the HS(*anti*) \rightarrow HS(*gau*) conformational switch, they readily undergo a spin switch that brings them to the LS(*gau*) configuration. In other words, the coupling between the conformational and the spin switches in the phase transition of **2** upon cooling arises from the fact that the intermediate phase generated after the conformational rearrangement is not thermodynamically stable at the temperature at which it is generated.

The coupling between the conformational change and the spin transition in the LT \rightarrow HT phase transition of **2** can be rationalized by means of similar arguments as those used in the paragraph above. Starting from the LS(*gau*) polymorph, there are two conceivable mechanisms for the phase transition in the heating mode: i) LS(*gau*) \rightarrow HS(*gau*) \rightarrow HS(*anti*), or ii) LS (*gau*) \rightarrow LS(*anti*) \rightarrow HS(*anti*). As explained above, the large HS-LS energy gap when the butyl chains are in their *gauche* conformation results in the LS(*gau*) polymorph being more stable than the HS(*gau*) polymorph over a broad range of temperatures that extends much beyond room temperature. This strongly suggests that the phase transition cannot be initiated by the spin transition, which means that the phase transition takes place via the second mechanism, that is to say, the conformational switch precedes the spin transition⁸⁸. The LS(*anti*) polymorph is not detected as an intermediate phase in the phase transition because the HS-LS gap substantially decreases when the butyl chains go from the *gauche* to the *anti* conformation. Due to this small gap, HS is the thermodynamically stable spin configuration at the temperature at which LS(*anti*) is generated (\sim 340 K), and,

therefore, the conformational switch is readily followed by a spin transition that brings the system to the HS(*anti*) polymorph.

Overall, our computational work offers new insights into the mechanism of the hysteretic phase transition of butyl-SBP. The phase transition of this material involves both a spin switch of its constituent π -dimers and a conformational switch of the butyl chains attached to these dimers. In both the heating and cooling modes of the phase transition, the conformational rearrangement of the butyl chains precedes the spin transition of the π -dimers. The spin transition occurs readily after the conformational change (i.e, without the detection of any intermediate phase) as a result of a coupling between the two types of switch, which arises from the strong dependence of the HS-LS energy gap of the π -dimers on the conformation adopted by the butyl chains. Given that the conformational rearrangement of the butyl chains is the first step in the phase transition of **2**, the onset of such phase transition is governed by the conformational energy landscape of the butyl chains in the crystal. Remarkably, the conformational energy landscape of the butyl chains in the LT phase of **2** (i.e, in the LS(*gau*) polymorph) is drastically different from that of the HT phase (i.e, the HS(*anti*) polymorph). This difference originates in the expansion of the crystal in going from LT to HT, which in turn is caused by the conformational change that brings the butyl chains from the *gauche*-IN conformation to an *anti* conformation. In fact, the butyl chains in HT exhibit dynamic disorder by virtue of the extra free space in the expanded crystal. The pronounced differences between the conformational energy landscapes of the butyl chains in the LT and HT phases are key to understanding the origin of the hysteresis observed in the phase transition of **2**. As displayed in Figure 7, the barrier that needs to be overcome to go from the *gauche*-IN to the *anti* conformer in LT is larger than the barrier that needs to be surmounted in going from the *anti* conformer to the *gauche*-IN conformer in HT. In addition, the energy separation between the two conformational minima is larger in LT (where the *gauche*-IN conformer is the most stable one) than in HT (where the *anti* conformer is the most stable one). For these reasons, the LT \rightarrow HT phase transition occurs at higher temperatures than the HT \rightarrow LT phase transition, thereby opening a hysteresis loop. The higher temperature of the phase transition in the heating mode is determined by the energetic cost associated with the *gauche*-IN \rightarrow *anti* conformational rearrangement and structural cooperative effects by virtue of which the conformational switch of a butyl chain facilitates the subsequent rotation of neighboring butyl chains.

Finally, it is worth commenting on the solid-state properties of the propyl-SBP radical, which also forms π -dimers in the solid state.⁴³ Given that the π -dimers of both ethyl-SBP and butyl-SBP feature spin-transitions, one might expect that the π -dimers of propyl-SBP should also present such behavior. However, magnetic susceptibility measurements showed that the dimers of propyl-SBP are in their HS state over the whole temperature range ($T > 30$ K), thus giving rise to a paramagnetic material without switching properties.⁴³ The adiabatic energy gap between the LS and HS minima, ΔE^{adia} , of the π -dimers of propyl-SBP in the solid state is -1.9 kcal/mol, which is considerably smaller than the ΔE^{adia} values for **1** and **2** (-2.6 and -9.5 kcal/mol, respectively). This small ΔE^{adia} value explains why the π -dimers of propyl-SBP remain in their HS state in the whole range of temperatures without undergoing any spin transition⁸⁹. The ΔE^{adia} value for an isolated π -dimer of propyl-SBP is significantly larger in absolute value (-2.7 kcal/mol) and very close to the ΔE^{adia} value found for ethyl-SBP, which means that the absence of any spin-transition in the material originates in solid-state effects. In order to get more insight into such effects, we carried out single point energy calculations of an isolated π -dimer excised from the optimized LS polymorph and an isolated π -dimer excised from the optimized HS polymorph. The difference in energy between these two π -dimers (-2.9 kcal/mol) is almost identical to the ΔE^{adia} value obtained in gas phase (-2.7 kcal/mol). This is not surprising in view of the fact that the structure of the π -dimers in the optimized polymorphs is very similar to the structure of the optimized isolated π -dimers (see Figure S4). It is thus concluded that the absence of any spin-transition in the butyl-SBP material is due to intermolecular interactions between π -dimers and not to the fact that crystal-packing effects impose a particular structure of the π -dimers that favors the HS state.

Conclusions

Our computational study on the phase transition of butyl-SBP puts the spotlight on the conformational changes of the butyl chains bonded to the N atoms of the superimposed PLY rings. Neither the thermodynamics of its phase transition nor its hysteretic behavior can be understood without considering the conformational degrees of freedom of the butyl groups. Indeed, the phase transition of butyl-SBP occurs at temperatures higher than room temperature because of the coupling of the spin-transition of its π -dimers with an order-disorder transition involving the butyl chains. This order-disorder transition in the heating mode is triggered by a rotation of the terminal methyl group of the butyl chains, which drives the methyl group from a *gauche* conformation (with respect to the methylene unit of the butyl bonded to the N atom of the superimposed PLY) to an *anti* conformation. The significant expansion of the crystal upon phase transition in the heating mode is due to this particular *gauche* \rightarrow *anti* conformational rearrangement. The phase transition of butyl-SBP is initiated via the conformational rearrangement of the butyl chains both upon heating and cooling. Such conformational switch is readily followed by the spin switch of the π -dimers due to the coupling between the two types of switch, which arises from the strong influence exerted by the conformation adopted by the butyl chains in the crystal on the energy difference between the high- and low-spin states of the π -dimers. In particular, this energy gap considerably decreases upon the *gauche* \rightarrow *anti* transition, which means that the crystal packing associated with the *anti* conformation tends to favor the high-spin states of the π -dimers, whereas the crystal packing associated with the *gauche* conformation tends to favor the low-spin states.

Our investigations reveal that the hysteresis observed in the phase transition of butyl-SBP originates in the fact that the conformational energy landscape of the butyl chains in the crystal lattice of the LT phase is completely different from that found in the crystal lattice of the HT phase. Specifically, the *gauche* \rightarrow *anti* conformational switch in the crystal lattice of LT entails a larger energy penalty, which is mainly due to the steric repulsion associated with a short H \cdots H contact between the terminal methyl group of a butyl chain in its *anti* conformation and the PLY ring of the adjacent SBP radical. The large energy penalty associated with this conformational switch and the strong structural cooperativity that assists the order-disorder transition of the butyl chains control the temperature at which the LT \rightarrow HT phase is initiated and, as a result, the width of the hysteresis loop.

The herein unveiled key role of the conformational changes of the butyl changes in controlling the phase transition of butyl-SBP not only provides a rationale for its intriguing and enigmatic bistable behavior but also provides valuable information that might serve for the rational design of new spirobiphenalenyl-based bistable materials. Transcending the specific material herein studied, our results highlight the great potential of coupling a conformational rearrangement of a flexible moiety with an electronic transition for the design and preparation of new bistable materials.

Computational details

All the electronic structure calculations performed in this work were carried out using the PBE exchange-correlation functional⁹⁰ within the spin-unrestricted formalism. The semiempirical dispersion potential introduced by Grimme⁹¹ was added to the conventional Kohn-Sham DFT energy in order to properly describe the van der Waals interactions. The parametrization employed in this work is the so-called DFT-D2. The use of PBE together with the Grimme correction is known to lead to good predictions for the structure and cohesive energies of molecular crystals.⁹² In the following, we provide further details of the methodology employed to obtain the results presented in each subsection of the *Results and Discussion*.

1) Phase transition of butyl-SBP: a spin transition coupled with a conformational rearrangement of the butyl groups.

The optimized structures of the LT and HT polymorphs were obtained by means of variable-cell geometry relaxations, in which the atomic positions and the lattice parameters are optimized simultaneously. Plane wave pseudopotential calculations using Vanderbilt ultrasoft pseudopotentials⁹³ and Γ -point sampling of the Brillouin zone were employed for these relaxations. In these calculations, the number of plane waves was kept constant at a kinetic energy cutoff of 60 Ry. A constant number of plane waves imply no Pulay stress but a decreasing precision of the calculation as the volume of the cell increases.⁹⁴ The large cutoff employed in these calculations ensures that the artifacts arising from this change of precision are negligible. The starting atomic positions and initial lattice parameters for the relaxation of the LS(*gau*) and HS (*anti*) polymorphs were taken from the X-ray resolved structures of the LT and HT phases of **2** at 100 and 360 K, respectively. For the relaxation of the LS(*anti*) and HS(*gau*) polymorphs, the same starting coordinates were used except for the initial dihedral angles defined for the butyl-ligands bonded to the sup-PLY units (θ), which were manually changed.

The optimizations of the isolated π -dimers of **2** (carried out with the goal of evaluating the gas-phase ΔE^{adia} values) were also done with plane wave pseudopotential calculations using Vanderbilt ultrasoft pseudopotentials. In these calculations, in which the plane wave basis set was expanded at a kinetic energy cutoff of 60 Ry, the π -

dimers were placed in a cell of 60-30-30 Bohr length sides trying to minimize the interactions between the equivalent images.

All the results presented in this subsection were obtained with the QUANTUM ESPRESSO package.⁹⁵

2) Origin of the main structural differences between the two polymorphs of 2.

The analysis presented in this subsection was done using the results obtained in the previous subsection

3) Driving forces of the phase transition of butyl-SBP. Order-disorder transition involving the butyl chains.

The vibrational entropy of the different polymorphs and the isolated π -dimers was evaluated after computing the vibrational frequencies of these systems in the harmonic approximation. The analytical frequencies of the isolated LS and HS π -dimers of **2** were computed using the re-optimized geometries obtained with the 6-31g(d) atomic basis⁹⁶ set within the Gaussian09 package.⁹⁷ For these optimizations, the previous optimized structures obtained with QUANTUM ESPRESSO were used as the initial atomic coordinates. The vibrational frequencies in the condensed phase were calculated by means of a finite-difference normal-mode analysis of the optimized structures. After the variable-cell relaxation of the HS(*anti*) and HS(*gau*) polymorphs at a cutoff of 60 Ry, the corresponding optimized atomic positions and optimized lattice parameters were used to define the initial geometries for a subsequent optimization at a cutoff of 45 Ry in which the lattice parameters were kept fixed. These new optimizations with a smaller cutoff were performed to be able to carry out finite-difference normal mode analysis of these two solid-state minima at a reasonable computational cost. It should be mentioned that switching from a cutoff of 60 Ry to a cutoff of 45 Ry results in negligible differences in both structures and energies of both polymorphs. It thus follows that the computational strategy has been properly set up.

The AIMD simulations were carried out using the efficient Car-Parinello propagation scheme⁹⁸ as implemented in the CPMD package.⁹⁹ In these simulations the plane wave basis set was expanded at a kinetic energy cutoff of 25 Ry. The molecular dynamics time step was set to 4 a.u. and the fictitious mass for the orbitals was chosen to be 400 a.u. All dynamic simulations were performed in the canonical ensemble using

the Nosé-Hoover chain thermostats¹⁰⁰ in order to control the kinetic energy of the nuclei and the fictitious kinetic energy of the orbitals. The lattice parameters employed in the AIMD simulations of the LT and HT phases at 340 K were taken directly from the X-ray crystals refined at 340 K of the LT and HT polymorphs, respectively. In the simulations of the LT phase, the electronic structure of the π -dimers was that corresponding to their singlet ground state. Conversely, in the simulations of the HT phase, the electronic structure of the π -dimers was that corresponding to their triplet ground state.

4) Origin of the hysteresis and the coupling between the spin transition and the conformational change in the phase transition of butyl-SBP

All the calculations of this section were performed using Vanderbilt ultrasoft pseudopotentials⁹³ and Γ -point sampling of the Brillouin zone.

The three profiles for the conformational rotation of the butyl ligand bonded to the supPLY unit (Figure 7) were evaluated by means of constrained optimizations in the solid state using three different sets of cell vectors to define the periodic boundary conditions: the cell vectors associated with the LT-340 crystal structure, the cell vectors of the HT-340 crystal structure and the cell vectors of LS(*gau*) polymorph, which were obtained upon variable-cell optimization (i.e., they correspond to the structure at 0 K). Nine constrained optimizations were performed for the first two profiles along the rotation coordinate of the θ dihedral angle fixing its value between -107° and $+107^\circ$. For the LS(*gau*) polymorph, in turn, five calculations were performed along the same rotation coordinate between the -107° and 0° values of the θ dihedral angle. These calculations were done using a kinetic energy cutoff of 35 Ry.

To study the elementary steps of the LS(*gau*) \rightarrow LS(*anti*) phase transition, the intermediate states connecting these two polymorphs (*3gauche-1anti*, *2gauche-2anti* and *1gauche-3anti*) were obtained by means of variable-cell geometry relaxations, in which the atomic positions and the lattice parameters are optimized simultaneously. In these calculations, the number of plane waves was kept constant at a kinetic energy cutoff of 60 Ry.

Supporting Information

Figure S1. X-ray crystal structures of the LT and HT phases of the ethyl and butyl radicals showing their characteristic crystal-packing motif: the π -dimers. **Figure S2.** Highest occupied molecular orbitals of the lowest singlet state (1A_g) and the triplet state (3A_u) of the π -dimer of butyl-SBP. **Figure S3.** Definition of the parameter that corresponds to the interplanar distance between sup-PLY units, and the parameter that corresponds to the CH $\cdots\pi$ distance depicted in the unit cell of the butyl-SBP system. **Figure S4.** Optimized structures of the π -dimers (both in the solid state and in the gas phase) of propyl-SBP. **Table S1.** Selected structural parameters for the SBP π -dimers present in two different X-ray crystal structures of ethyl-SBP and the corresponding structural parameters obtained upon geometry optimization of these SBP π -dimers in their 1A_g and 3A_u states. **Table S2.** Cell parameters of the reported LT-340 and HT-340 X-ray crystal structures of **2**. **Table S3.** Cell parameters of the LT-0 minimum energy structure of butyl-SBP and of the LT crystallographic structures resolved at 100 and 340 K. **Table S4.** Potential energy of the butyl substituted SBP crystallographic unit cell at 0K when considering the rotation from -107° (*gauche*) to 0° (*anti*) of one N-linked butyl ligand and the corresponding unit cell distortion. **Supporting Note 1.** Detailed explanation of how the cooperativity of the LS(*gau*) \rightarrow LS(*anti*) phase transition was assessed.

Acknowledgments

We acknowledge the Spanish Government for financial support (Projects MAT2011-25972 and MAT2014-54025-P) and a “Ramón y Cajal” fellowship to J.R.-A. We also acknowledge Universitat de Barcelona for a Ph.D grant to M.F, and BSC and CSUC for the allocation of massive computer time. We are also thankful to the Catalan DURSI (Grant 2014SGR1422). Finally, we would also like to thank Dr. Sergi Vela for helping us with assessing the cooperativity of the phase transition of **2**.

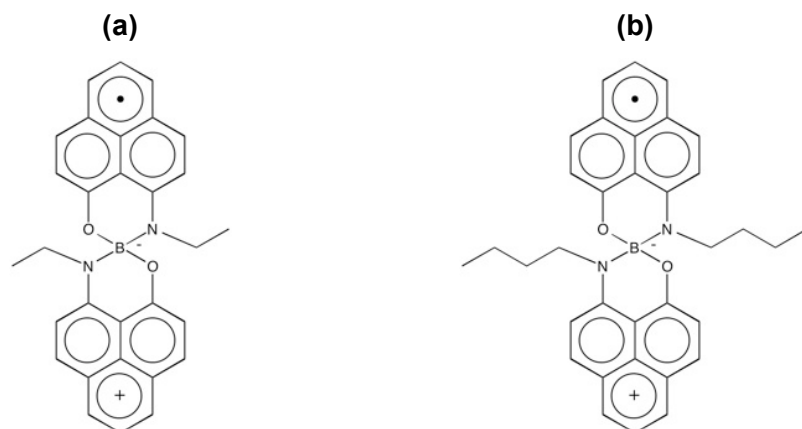


Figure 1. Schemes of the ethyl-substituted (a) and the butyl-substituted (b) N- and O-functionalized spiro-bis(1,9-disubstitutedphenalenyl) boron radicals. The radical displayed on the left (right) is referred to as compound **1** (**2**) in the text.

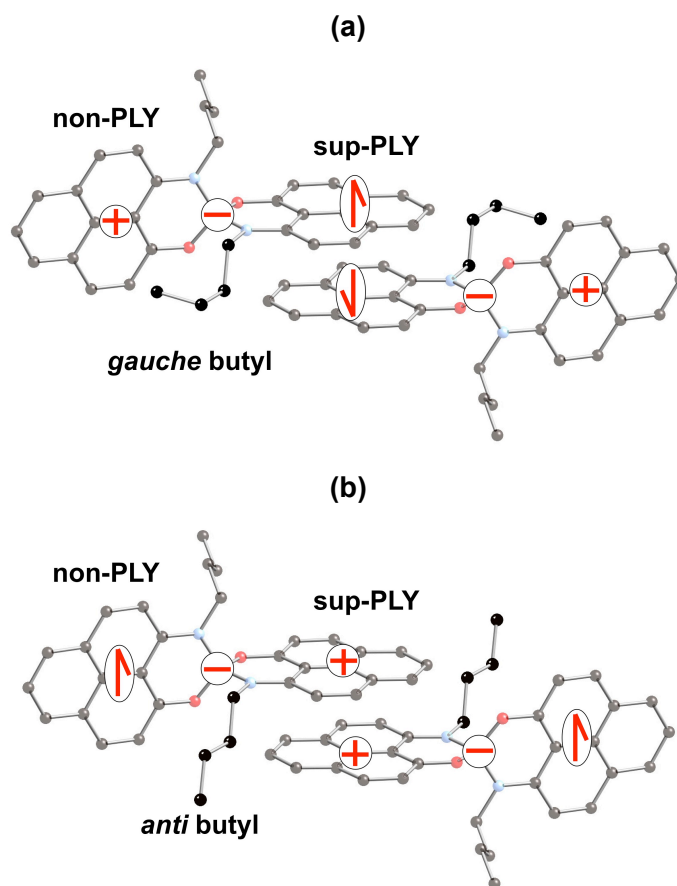


Figure 2. X-ray crystal structures at 340 K of the LT (a) and HT (b) phases of the butyl-SBP π -dimers. Hydrogen atoms are hidden for clarity.

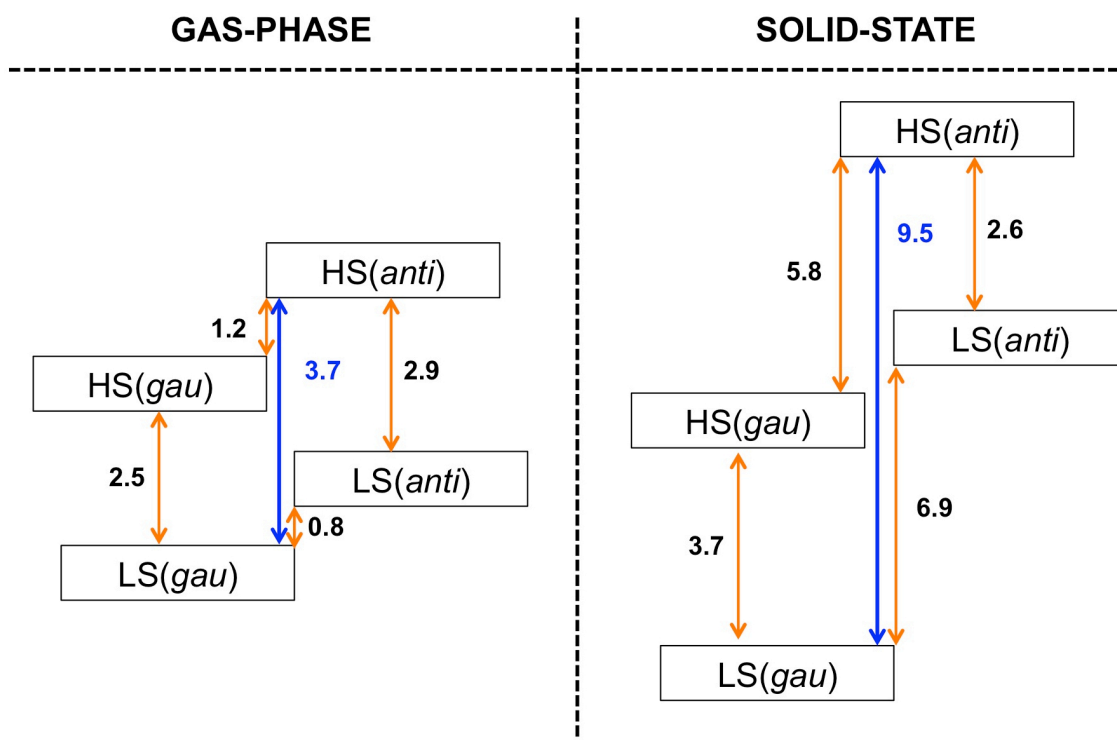


Figure 3. Scheme of the relative energy of the different minimum energy configurations of compound **2** in gas phase (left) and solid-state (right). All adiabatic energy gaps are given, per π -dimer, in kcal/mol.

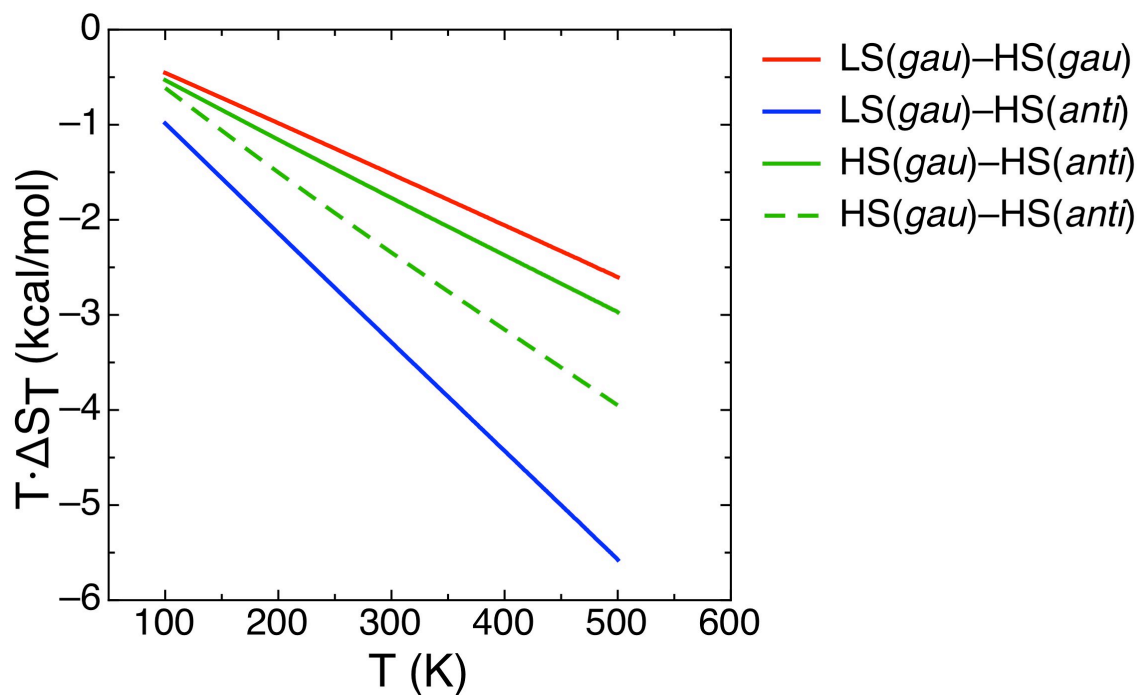


Figure 4. Temperature dependence of the difference in entropy (expressed as $T\Delta S_T$, where ΔS_T includes both the electronic and vibrational contributions of the entropy) between different configurations of the π -dimers of **2**. The solid curves correspond to calculations carried out for isolated π -dimers, while the dashed curve corresponds to calculations in the solid state.

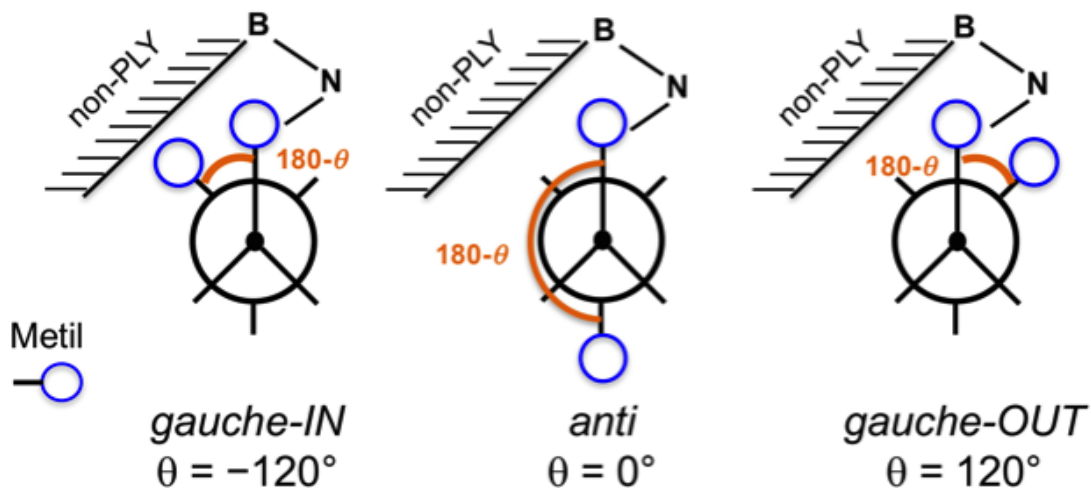


Figure 5. Scheme for the *gauche-IN*, *anti* and *gauche-OUT* conformations of the butyl chain of compound **2**.

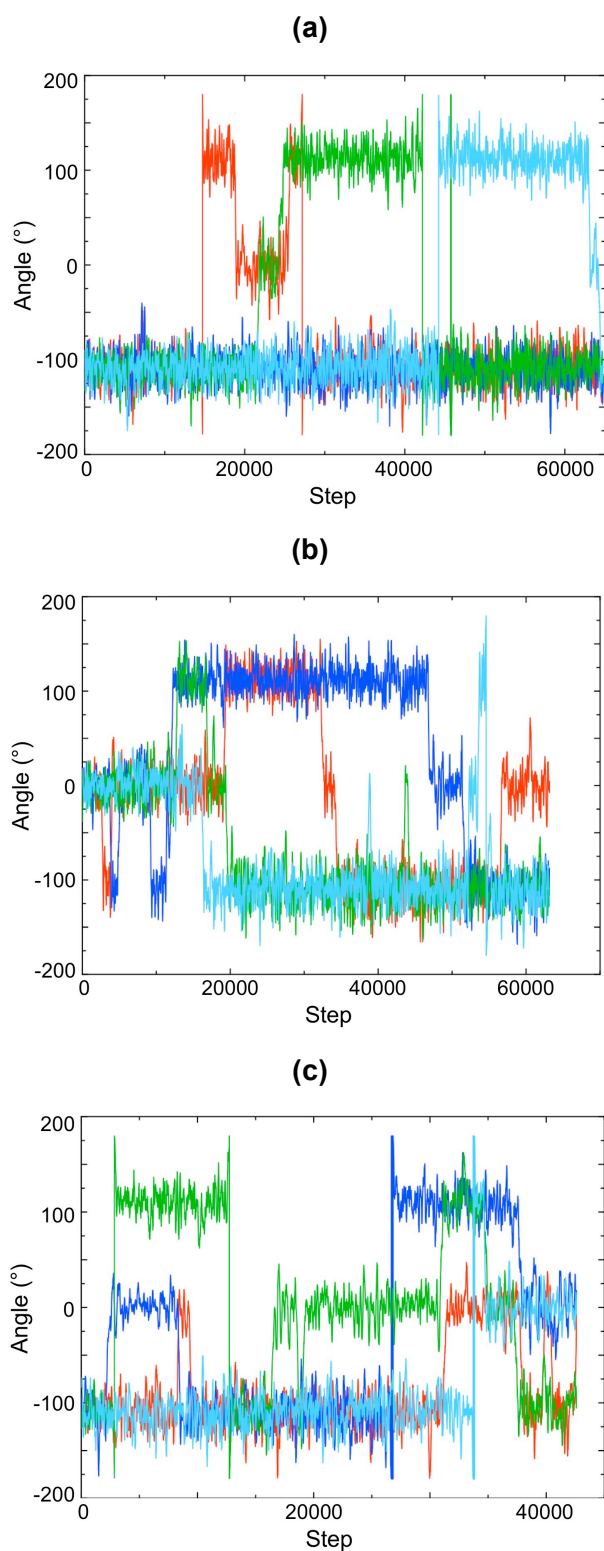


Figure 6. Time-resolved evolution of the θ dihedral angle of the butyl-ligands attached to the sup-PLY (see Figure 5) for the four spiro-phenalenyl units included in the cell of the AIMD simulations. The values that correspond to the trajectory of the LT-340 (LS) phase are shown in **(a)**, whereas **(b)** and **(c)** show the values for the HT-340 (HS) trajectories, starting from *anti* and *gauche-IN* polymorphs, respectively. Note that in our simulations 10000 steps amount to *ca.* 10 picoseconds.

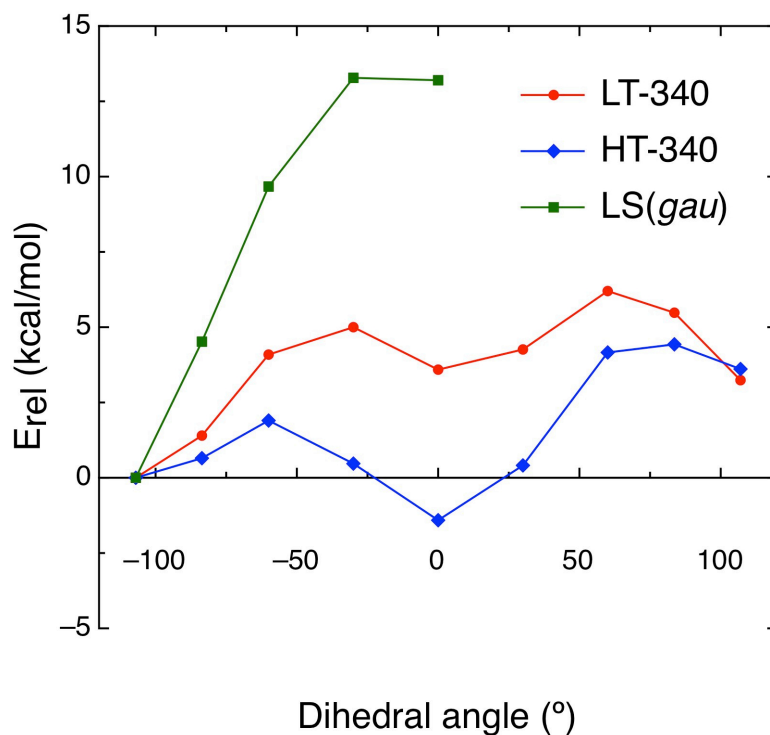


Figure 7. Potential energy profiles as a function of the θ dihedral angle of one butyl chain of the unit cell of **2**. The three profiles were evaluated by means of constrained optimizations using three different sets of cell vectors: the cell vectors associated with the LT-340 crystal structure (red curve), the cell vectors of the HT-340 crystal structure (blue curve) and the cell vectors of LS(*gau*) polymorph (green curve), which were obtained upon variable-cell optimization (i.e., they correspond to the structure at 0 K). In all profiles, the energy of the *gauche*-IN conformation ($\theta = -107^\circ$) was taken as the reference energy.

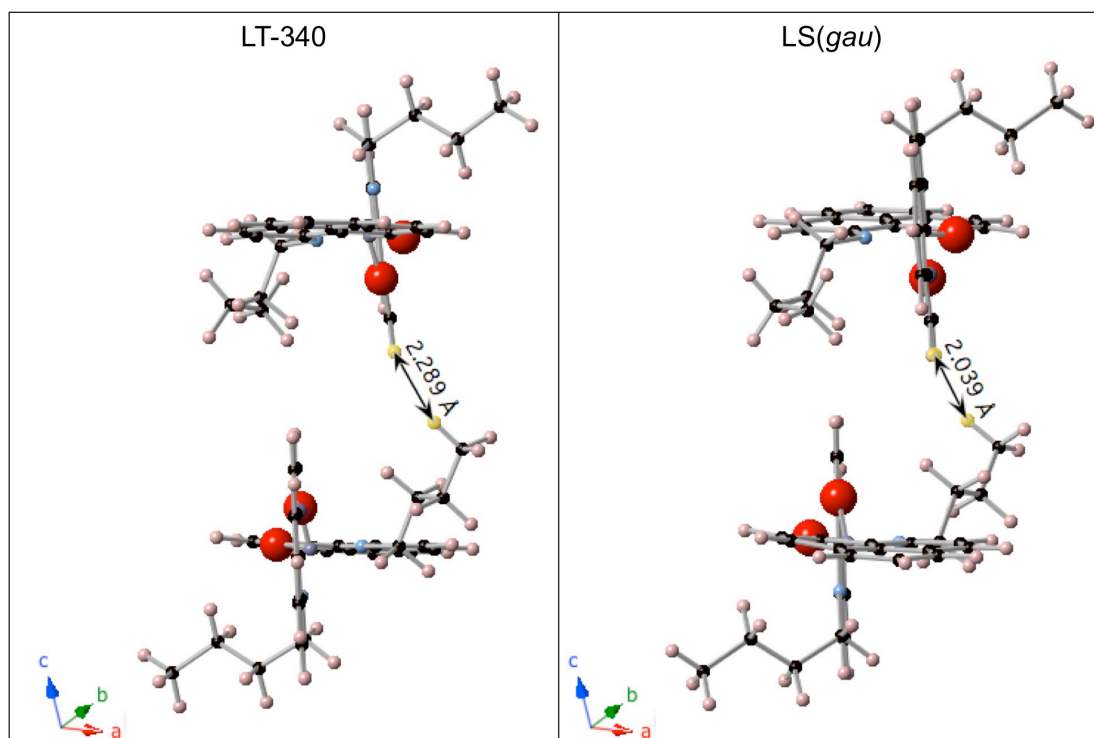


Figure 8. A short H···H contact between a hydrogen atom of the terminal methyl group of a butyl chain in an *anti* conformation and a hydrogen atom of a phenalenyl group of an adjacent SBP radical. The distance associated with this contact is shown for the LT-340 crystal structure (*left*) and for the optimized LS(*gau*) structure (*right*), i.e., the LT structure at 0 K. The values of the distances displayed in the Figure correspond to optimized structures. In the LT-340 case, one of the butyl chains was rotated to an *anti* conformation and all the atomic coordinates were allowed to relax while keeping the X-ray cell parameters of the LT-340 crystal structure. In the LS(*gau*) case, one of the butyl chains was rotated to an *anti* conformation and all the atomic coordinates were allowed to relax while keeping the cell parameters obtained from a previous variable-cell optimization in which no butyl chain was manually rotated to an *anti* conformation.

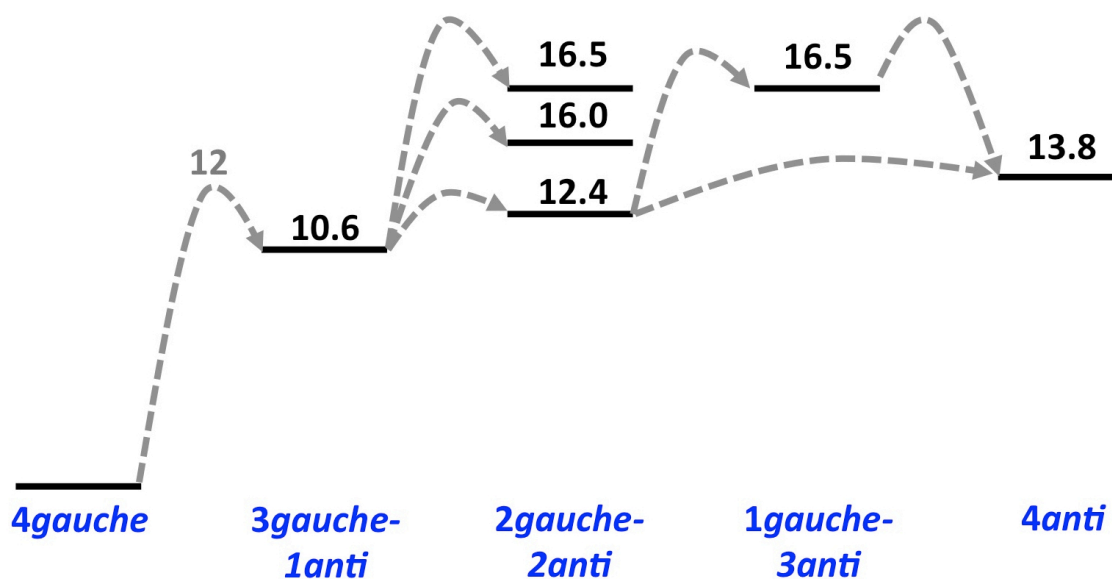


Figure 9. Scheme showing the energy changes (given in kcal/mol) involved in all the elementary steps of the LS(*gau*) \rightarrow LS(*anti*) phase transition. In LS(*gau*), which is denoted by “4*gauche*” in the Figure, there are four butyl groups in the *gauche*-IN conformation in the simulation cell. In LS(*anti*), which is denoted by “4*anti*” in the Figure, all the butyl chains adopt an *anti* conformation. The name employed to define the intermediate states connecting these two polymorphs denote how many butyl groups of those four originally adopting a *gauche*-IN conformation are still in a *gauche*-IN conformation and how many of them have switched to an *anti* conformation. Note that the second intermediate state actually comprises three different states because there are three different configurations with two butyls in a *gauche*-IN conformation and two butyls in an *anti* conformation. All the energies are given relative to the optimized structure of the LS(*gau*) polymorph.

Table 1. Selected structural parameters for the SBP π -dimers present in **(a)** the X-ray crystal structures of butyl-SBP at two different temperatures and the corresponding structural parameters obtained upon geometry optimization of these SBP π -dimers in their 1A_g and 3A_u states in **(b)** solid-state and in **(c)** gas-phase conditions. All distances are given in Angstrom.

	(a) X-Ray	(b) SS	(c) GP
	100K	LS (1A_g)	LS (1A_g)
D^a	3.193	3.157	3.210
C-N (S) ^b	1.369	1.362	1.362
C-O (S)	1.352	1.343	1.343
C-N (NS)	1.336	1.349	1.356
C-O (NS)	1.330	1.336	1.335
	360K	HS (3A_u)	HS (3A_u)
D	3.489	3.281	3.297
C-N (S)	1.328	1.350	1.355
C-O (S)	1.327	1.338	1.338
C-N (NS)	1.377	1.360	1.361
C-O (NS)	1.365	1.342	1.341

^a D refers to the interplanar distance between the superimposed PLYs. D has been measured as the distance between the central carbon (i.e., the carbon atom shared by the three fused benzene rings) of the two superimposed PLYs.

^b C-N (S) and C-N (NS) denote the C-N bond distance of the superimposed and nonsuperimposed PLYs, respectively. C-O (S) and C-O (NS) denote the C-O bond distance of the superimposed and nonsuperimposed PLY rings, respectively.

Table 2. (a) Volume cell (V), $\text{CH}\cdots\pi$ distance, and interplanar distance between sup-PLYs (D) obtained for the butyl-SBP crystal at the optimized *gauche*-IN and *anti* structures in their 1A_g and 3A_u states in solid-state conditions. All distances are given in Angstrom and the volume cell is given in bohr³. (b) Difference between the V , $\text{CH}\cdots\pi$, and D values of various polymorphs of the butyl-SBP crystal.

(a) Absolute values				
	LS(<i>gau</i>)	LS(<i>anti</i>)	HS(<i>gau</i>)	HS(<i>anti</i>)
V	2357.7438	2456.9682	2370.5952	2465.7967
$\text{CH}\cdots\pi$	2.575	2.688	2.590	2.700
D	3.154	3.206	3.238	3.281
(b) Differences				
	LS(<i>anti-gau</i>)^a	HS(<i>anti-gau</i>)^b	HS-LS(<i>gau</i>)^c	HS-LS(<i>anti</i>)^d
V	4.04%	3.86%	0.54%	0.36%
$\text{CH}\cdots\pi$	0.113	0.110	0.015	0.012
D	0.052	0.043	0.084	0.075

^a Difference between the LS(*anti*) and LS(*gau*) polymorphs

^b Difference between the HS(*anti*) and HS(*gau*) polymorphs

^c Difference between the HS(*gau*) and LS(*gau*) polymorphs

^d Difference between the HS(*anti*) and LS(*anti*) polymorphs

References

- ¹ O.Kahn and J.P. Launay, *Chemtronics* **1988**, *3*, 140-151.
- ² O. Sato, J. Tao and Y.Z. Zhang, *Angew. Chem., Int. Ed.* **2007**, *46*, 2152-2187.
- ³ R.G. Hicks, *Nat. Chem.* **2011**, *3*, 189-191.
- ⁴ *Spin-Crossover Materials-Properties and Applications*; M.A. Halcrow, Ed.; John Wiley & Sons: Hoboken, NJ, 2013.
- ⁵ O. Sato, *Nat. Chem.* **2016**, *8*, 644-656.
- ⁶ J. Kröber, E. Coddjovi, O. Kahn, F. Grolière and C. Jay, *J. Am. Chem. Soc.*, **1993**, *115*, 9810-9811.
- ⁷ V. Niel, J.M. Martínez-Agudo, M.C. Muñoz, A.B. Gaspar and J.A. Real, *Inorg. Chem.* **2001**, *40*, 3838-3839.
- ⁸ *Spin Crossover in Transition Metal Compounds I-III*, P. Gütlich and H. A. Goodwin, Ed. *Top. Curr. Chem.*, Springer-Verlag, Berlin, **2004**, vol. 233-235.
- ⁹ O. Jeannin, R. Clérac and M. Fourmigué, *J. Am. Chem. Soc.* **2006**, *128*, 14649-14656.
- ¹⁰ E. Coronado, J.R. Galán-Mascarós, M. Monrabal-Capilla, J. García-Martínez, P. Pardo-Ibáñez. *Adv. Mater.* **2007**, *19*, 1359.
- ¹¹ M. Nihei, H. Tahira, N. Takahashi, Y. Otake, Y. Yamamura, K. Saito and H. Oshio, *J. Am. Chem. Soc.* **2010**, *132*, 3553-3560.
- ¹² H.B. Duan, X.R. Chen, H. Yang, X.M. Ren, F. Xuan and S.M. Zhou, *Inorg. Chem.* **2013**, *52*, 3870-3877.
- ¹³ T. Romero-Morcillo, M. Seredyuk, M.C. Muñoz and J.A. Real, *Angew. Chem. Int. Ed.* **2015**, *54*, 14777-14781.
- ¹⁴ V. Gómez, C. Sáenz de Pipaón, P. Maldonado-Illescas, J.C. Waerenborgh, E. Martin, J. Benet-Buchholz and J.R. Galán-Mascarós, *J. Am. Chem. Soc.* **2015**, *137*, 11924-11927.
- ¹⁵ W. Fujita and K. Awaga, *Science* **1999**, *286*, 261-262.
- ¹⁶ M.E. Itkis, X. Chi, A.W. Cordes and R.C. Haddon, *Science* **2002**, *296*, 1443-1445.
- ¹⁷ J.L. Brusso, O.P. Clements, R.C. Haddon, M.E. Itkis, A.A. Leitch, R.T. Oakley, R.W. Reed and J.F. Richardson, *J. Am. Chem. Soc.* **2004**, *126*, 8256-8265.
- ¹⁸ J.L. Brusso, O.P. Clements, R.C. Haddon, M.E. Itkis, A.A. Leitch, R.T. Oakley, R.W. Reed and J.F. Richardson, *J. Am. Chem. Soc.* **2004**, *126*, 14692-14693.
- ¹⁹ K. Lekin, S.M. Winter, L.E. Downie, X.Z. Bao, J.S. Tse, S. Desgreniers, R.A. Secco, P.A. Dube and R.T. Oakley, *J. Am. Chem. Soc.* **2010**, *132*, 16212-16224.
- ²⁰ H. Phan, K. Lekin, S.M. Winter, R.T. Oakley and M. Shatruk, *J. Am. Chem. Soc.* **2013**, *135*, 15674-15677.

-
- ²¹ K. Lekin, H. Phan, S.M. Winter, J.W.L. Wong, A.A. Leitch, D. Laniel, W. Yong, R.A. Secco, J.S. Tse, S. Desgreniers, P.A. Dube, M. Shatruk and R.T. Oakley, *J. Am. Chem. Soc.* **2014**, *136*, 8050-8062.
- ²² T. Li, G. Tan, D. Shao, J. Li, Z. Zhang, Y. Song, Y. Sui, S. Chen, Y. Fang and X. Wang. *J. Am. Chem. Soc.* **2016**, *138*, 10092–10095.
- ²³ I. Ratera, D. Ruiz-Molina, F. Renz, J. Ensling, K. Wurst, C. Rovira, P. Gutlich and J. Veciana, *J. Am. Chem. Soc.* **2003**, *125*, 1462–1463.
- ²⁴ G. D'Avino, L. Grisanti, J. Guasch, I. Ratera, J. Veciana and A. Painelli, *J. Am. Chem. Soc.* **2008**, *130*, 12064-12072.
- ²⁵ H. Miyasaka, N. Motokawa, T. Chiyo, M. Takemura, M. Yamashita, H. Sagayama and T. Arima, *J. Am. Chem. Soc.* **2011**, *133*, 5338-5345.
- ²⁶ M. Mitsumi, T. Nishitani, S. Yamasaki, N. Shimada, Y. Komatsu, K. Toriumi, Y. Kitagawa, M. Okumura, Y. Miyazaki, N. Górska, A. Inaba, A. Kanda and N. Hanasaki, *J. Am. Chem. Soc.* **2014**, *136*, 7026-7037.
- ²⁷ A. Lannes, Y. Suffren, J.B. Tommasino, R. Chiriac, F. Toche, L. Khrouz, F. Molton, C. Duboc, I. Kieffer, J.L. Hazemann, C. Reber, A. Hauser, D. Luneau. *J. Am. Chem. Soc.* **2016**, *138*, 16493-16501.
- ²⁸ J. Tao, H. Maruyama and O. Sato *J. Am. Chem. Soc.* **2006**, *128*, 1790-1791.
- ²⁹ R.D. Schmidt, D.A. Shultz, J.D. Martin and P.D. Boyle, *J. Am. Chem. Soc.* **2010**, *132*, 6261-6273.
- ³⁰ N. Hoshino, F. Lijima, G.N. Newton, N. Yoshida, T. Shiga, H. Nojiri, A. Nakao, R. Kumai, Y. Murakami and H. Oshio, *Nat. Chem.* **2012**, *4*, 921-926.
- ³¹ X-H. Zhao, X-C. Huang, S-L. Zhang, D. Shao, H-Y. Wei and X-Y. Wang, *J. Am. Chem. Soc.* **2013**, *135*, 16006-16009.
- ³² P-P. Shi, Q. Ye, Q. Li, H-T. Wang, D-W. Fu, Y. Zhang and R-G. Xiong, *Chem. Mater.* **2014**, *26*, 6042-6049.
- ³³ Z-S. Yao, M. Mito, T. Kamachi, Y. Shiota, K. Yoshizawa, N. Azuma, Y. Miyazaki, K. Takahashi, K. Zhang, T. Nakanishi, S. Kang, S. Kanegawa and O. Sato, *Nat. Chem.* **2014**, *6*, 1079-1083.
- ³⁴ R.C. Haddon, *Nature* **1975**, *256*, 394-396.
- ³⁵ Y. Morita, S. Suzuki, K. Sato and T. Takui, *Nat. Chem.* **2011**, *3*, 197-204.
- ³⁶ S. Nishida, Y. Morita, K. Fukui, K. Sato, D. Shiomi, T. Takui and K. Nakasuji, *Angew. Chem. Int. Ed.* **2005**, *44*, 7277-7280.
- ³⁷ K.V. Raman, A.M. Kamerbeek, A. Mukherjee, N. Atodiresei, T.K. Sen, P. Lazic, V. Caciuc, R. Michel, D. Stalke, S.K. Mandal, S. Blugel, M. Munzenberg, J.S. Moodera, *Nature* **2013**, *493*, 509-513.
- ³⁸ A. Ueda, S. Suzuki, K. Yoshida, K. Fukui, K. Sato, T. Takui, K. Nakasuji and Y. Morita, *Angew. Chem. Int. Ed.* **2013**, *52*, 4795-4799.

-
- ³⁹ S.K. Pal, M.E. Itkis, F.S. Tham, R.W. Reed, R.T. Oakley and R.C. Haddon, *Science* **2005**, *309*, 281-284.
- ⁴⁰ Y. Morita, S. Suzuki, K. Fukui, S. Nakazawa, H. Kitagawa, H. Kishida, H. Okamoto, A. Naito, A. Sekine, Y. Ohashi, M. Shiro, K. Sasaki, D. Shiomi, K. Sato, T. Takui and K. Nakasuji, *Nat. Mater.* **2008**, *7*, 48-51.
- ⁴¹ X. Chi, M.E. Itkis, B.O. Patrick, T.M. Barclay, R.W. Reed, R.T. Oakley, A.W. Cordes, and R.C. Haddon, *J. Am. Chem. Soc.* **1999**, *121*, 10395-10402.
- ⁴² X. Chi, M.E. Itkis, K. Kirschbaum, A.A. Pinkerton, R.T. Oakley, A.W. Cordes and R.C. Haddon, *J. Am. Chem. Soc.* **2001**, *123*, 4041-4048.
- ⁴³ X. Chi, M.E. Itkis, R.W. Reed, R.T. Oakley, A.W. Cordes and R.C. Haddon, *J. Phys. Chem. B* **2002**, *106*, 8278-8287.
- ⁴⁴ X. Chi, M.E. Itkis, F.S. Tham, R.T. Oakley, A.W. Cordes and R.C. Haddon, *Int. J. Quant. Chem.* **2003**, *95*, 853-865.
- ⁴⁵ X. Chi, F.S. Tham, A.W. Cordes, M.E. Itkis, and R.C. Haddon, *Synth. Met.* **2003**, *133-134*, 367-372.
- ⁴⁶ P. Liao, M.E. Itkis, R.T. Oakley, F.S. Tham and R.C. Haddon, *J. Am. Chem. Soc.* **2004**, *126*, 14297-14302.
- ⁴⁷ S.K. Pal, M.E. Itkis, R.W. Reed, R.T. Oakley, A.W. Cordes, F.S. Tham, T. Siegrist and R.C. Haddon, *J. Am. Chem. Soc.* **2004**, *126*, 1478-1484.
- ⁴⁸ S.K. Mandal, M.E. Itkis, X. Chi, S. Samanta, D. Lidsky, R.W. Reed, R.T. Oakley, F.S. Tham and R.C. Haddon, *J. Am. Chem. Soc.* **2005**, *127*, 8185-8196.
- ⁴⁹ S.K. Mandal, S. Samanta, M.E. Itkis, D.W. Jensen, R.W. Reed, R.T. Oakley, F.S. Tham, B. Donnadieu and R.C. Haddon, *J. Am. Chem. Soc.* **2006**, *128*, 1982-1994.
- ⁵⁰ S.K. Pal, M.E. Itkis, F.S. Tham, R.W. Reed, R.T. Oakley, B. Donnadieu and R.C. Haddon, *J. Am. Chem. Soc.* **2007**, *129*, 7163-7174.
- ⁵¹ A. Sarkar, S.K. Pal, M.E. Itkis, P. Liao, F.S. Tham, B. Donnadieu and R.C. Haddon, *Chem. Mater.* **2009**, *21*, 2226-2237.
- ⁵² P. Bag, M.E. Itkis, S.K. Pal, B. Donnadieu, F.S. Tham, H. Park, J.A. Schlueter, T. Siegrist and R.C. Haddon, *J. Am. Chem. Soc.* **2010**, *132*, 2684-2694.
- ⁵³ A. Sarkar, S.K. Pal, M.E. Itkis, F.S. Tham and R.C. Haddon, *J. Mat. Chem.* **2012**, *22*, 8245-8256.
- ⁵⁴ A. Sarkar, M.E. Itkis, F.S. Tham and R.C. Haddon, *Chem. Eur. J.* **2011**, *17*, 11576-11584.
- ⁵⁵ P. Bag, S.K. Pal, M.E. Itkis, A. Sarkar, F.S. Tham, B. Donnadieu and R.C. Haddon, *J. Am. Chem. Soc.* **2013**, *135*, 12936-12939.
- ⁵⁶ S.K. Pal, P. Bag, M.E. Itkis, F.S. Tham and R.C. Haddon, *J. Am. Chem. Soc.* **2014**, *136*, 14738-14741.

-
- ⁵⁷ P. Bag, M.E. Itkis, D. Stekovic, S.K. Pal, F.S. Tham and R.C. Haddon, *J. Am. Chem. Soc.* **2015**, *137*, 10000-10008.
- ⁵⁸ S.K. Pal, P. Bag, A. Sarkar, X. Chi, M.E. Itkis, F.S. Tham, B. Donnadiu and R.C. Haddon, *J. Am. Chem. Soc.* **2010**, *132*, 17258-17264.
- ⁵⁹ R.C. Haddon, A. Sarkar, S.K. Pal, X. Chi, M.E. Itkis and F.S. Tham, *J. Am. Chem. Soc.* **2008**, *130*, 13683-13690.
- ⁶⁰ J. Huang and M. Kertesz, *J. Am. Chem. Soc.* **2003**, *125*, 13334-13335.
- ⁶¹ J. Huang and M. Kertesz, *J. Phys. Chem. A* **2007**, *111*, 6304-6315.
- ⁶² T. Taniguchi, T. Kawakami and K. Yamaguchi, *Polyhedron* **2005**, *24*, 2274-2279.
- ⁶³ M. Takenaka, T. Taniguchi, T. Kawakami, Y. Kitagawa, M. Okumura and K. Yamaguchi, *Chem. Lett.* **2007**, *36*, 1000-1001.
- ⁶⁴ M. Fumanal, F. Mota, J.J. Novoa and J. Ribas-Arino, *J. Am. Chem. Soc.* **2015**, *137*, 12843-12855.
- ⁶⁵ Y. Takano, T. Taniguchi, H. Isobe, T. Kubo, Y. Morita, K. Yamamoto, K. Nakasuji, T. Takui and K. Yamaguchi, *J. Am. Chem. Soc.* **2002**, *124*, 11122-11130.
- ⁶⁶ D. Small, V. Zaitsev, Y. Jung, S.V. Rosokha, M. Head-Gordon and J.K. Kochi, *J. Am. Chem. Soc.* **2004**, *126*, 13850-13858.
- ⁶⁷ F. Mota, J.S. Miller and J.J. Novoa, *J. Am. Chem. Soc.* **2009**, *131*, 7699-7707.
- ⁶⁸ S. Suzuki, Y. Morita, K. Fukui, K. Sato, D. Shiomi, T. Takui and K. Nakasuji, *J. Am. Chem. Soc.* **2006**, *128*, 2530-2531.
- ⁶⁹ D. Small, S.V. Rosokha, J.K. Kochi and M. Head-Gordon, *J. Phys. Chem. A* **2005**, *109*, 11261.
- ⁷⁰ V. Zaitsev, S.V. Rosokha, M. Head-Gordon and J.K. Kochi, *J. Org. Chem.* **2006**, *71*, 520.
- ⁷¹ J. Huang and M. Kertesz, *J. Am. Chem. Soc.* **2006**, *128*, 1418-1419.
- ⁷² J. Huang and M. Kertesz, *J. Am. Chem. Soc.* **2007**, *129*, 1634-1643.
- ⁷³ Y.-H. Tian and M. Kertesz, *J. Am. Chem. Soc.* **2010**, *132*, 10648-10649.
- ⁷⁴ Kolb, B.; Kertesz, M.; Thonhauser, T. *J. Phys. Chem. A* **2013**, *117*, 3642-3649.
- ⁷⁵ Z. Cui, H. Lischka, H.Z. Beneberu and M. Kertesz, *J. Am. Chem. Soc.* **2014**, *136*, 5539-5542.
- ⁷⁶ Z. Mou, K. Uchida, T. Kubo and M. Kertesz, *J. Am. Chem. Soc.* **2014**, *136*, 18009-18022.
- ⁷⁷ Y-H. Tian, B.G. Sumpter, S. Du and J. Huang, *J. Phys. Chem. Lett.* **2015**, *6*, 2318-2325.
- ⁷⁸ Z. Mou, T. Kubo and M. Kertesz, *Chem. Eur. J.* **2015**, *21*, 18230-18236.
- ⁷⁹ B. Le Guennic, S. Borshch, V. Robert. *Inorg. Chem.* **2007**, *46*, 11106-11111.

-
- ⁸⁰ M. Kepenekian, B. Le Guennic, V. Robert. *Phys. Rev. B* **2009**, *79*, 094428.
- ⁸¹ S. Vela, M. Fumanal, J. Ribas-Arino, V. Robert. *Phys. Chem. Chem. Phys.* **2015**, *17*, 16306-16314.
- ⁸² This particular energetic ordering is opposite to the ordering found in an isolated *n*-butane molecule. It is thus inferred that the intramolecular interaction between the non-PLY and the ending methyl stabilizes the *gauche*-IN conformer in front of the *anti* one.
- ⁸³ The ΔE^{adia} value between both *gauche*-IN LS and HS minima is *ca.* 1 kcal/mol larger than the ΔE^{adia} value between *anti* polymorphs (see Figure 3). We ascribe the larger adiabatic gap to the shorter interplanar distance adopted by the sup-PLY units in the *gauche*-IN polymorph (see Table 2 to compare the geometrical parameters of the *gauche*-IN and *anti* minima), which results in a relative stabilization of the LS state by virtue of a larger SOMO-SOMO overlap.
- ⁸⁴ H. Bolvin, O. Kahn. *Chem. Phys.* **1995**, *192*, 295-305.
- ⁸⁵ C.P. Slichter, H.G. Drickamer. *J. Chem. Phys.* **1972**, *56*, 2142-2160.
- ⁸⁶ H. Paulsen. *Magnetochemistry*. **2016**, *2*, 14.
- ⁸⁷ M. Kepenekian, B. Le Guennic, V. Robert. *J. Am. Chem. Soc.* **2009**, *131*, 11498-11502.
- ⁸⁸ Note that the energy gap between LS(*anti*) and LS(*gau*) is larger than the energy gap between HS(*gau*) and LS(*gau*) (see Figure 3). It thus would appear that it is easier for the system to undergo a spin switch than a conformational switch. In this sense, it could be argued that the spin switch should occur prior to the conformational switch in the LT \rightarrow HT phase transition. However, the conformational switch entails an order-disorder transition that brings about a large increase in the vibrational entropy of the system. Such an increase in the vibrational entropy upon conformational switch is much larger than that associated with the spin switch. Therefore, the large increase in vibrational entropy associated with the conformational switch explains why the system undergo first the conformational switch even if the energy gap that is cleared in this transition is larger than that of the spin switch.
- ⁸⁹ Note that the electronic and vibrational entropy of the HS state is larger than that of the LS state. This is why the π -dimers of propyl-SBP remain in the HS over the whole range of temperatures even if the HS state lies slightly above in energy than the LS state.
- ⁹⁰ (a) J.P. Perdew, K. Burke and M. Ernzerhof, *Phys. Rev. Lett.* **1996**, *77*, 3865–3868 (b) J.P. Perdew, K. Burke and M. Ernzerhof, *Phys. Rev. Lett.* **1997**, *78*, 1396.
- ⁹¹ S. Grimme, *J. Comput. Chem.* **2006**, *27*, 1787–1799.
- ⁹² T. Bucko, J. Hafner, S. Lebègue and J. Ángyán, *J. Phys. Chem. A* **2010**, *114*, 11814–11824.
- ⁹³ D. Vanderbilt, *Phys. Rev. B* **1990**, *41*, 7892–7895.
- ⁹⁴ D. Marx and J. Hutter, *Ab Initio Molecular Dynamics: Basic Theory and Advanced Methods* (Cambridge Univ. Press, **2009**).
- ⁹⁵ P. Giannozzi, S. Baroni, N. Bonini, M. Calandra, R. Car, C. Cavazzoni, D. Ceresoli, G.L. Chiarotti, M. Cococcioni, I. Dabo, A. Dal Corso, S. Fabris, G. Fratesi, S. de Gironcoli, R.

Gebauer, U. Gerstmann, C. Gougoussis, A. Kokalj, M. Lazzeri, L. Martin-Samos, N. Marzari, F. Mauri, R. Mazzarello, S. Paolini, A. Pasquarello, L. Paulatto, C. Sbraccia, S. Scandolo, G. Scalzero, A.P. Seitsonen, A. Smogunov, P. Umari and R.M. Wentzcovitch, *J. Phys. Condens. Matter*, **2009**, *21*, 395502. (Quantum ESPRESSO v. 4.2.1).

⁹⁶ R. Ditchfield, W.J. Hehre and J.A. Pople, *J. Chem. Phys.* **1971**, *54*, 724.

⁹⁷ Gaussian 09, Revision **D.01**, M. J. Frisch, G. W. Trucks, H. B. Schlegel, G. E. Scuseria, M. A. Robb, J. R. Cheeseman, G. Scalmani, V. Barone, B. Mennucci, G. A. Petersson, H. Nakatsuji, M. Caricato, X. Li, H. P. Hratchian, A. F. Izmaylov, J. Bloino, G. Zheng, J. L. Sonnenberg, M. Hada, M. Ehara, K. Toyota, R. Fukuda, J. Hasegawa, M. Ishida, T. Nakajima, Y. Honda, O. Kitao, H. Nakai, T. Vreven, J. A. Montgomery, Jr., J. E. Peralta, F. Ogliaro, M. Bearpark, J. J. Heyd, E. Brothers, K. N. Kudin, V. N. Staroverov, R. Kobayashi, J. Normand, K. Raghavachari, A. Rendell, J. C. Burant, S. S. Iyengar, J. Tomasi, M. Cossi, N. Rega, J. M. Millam, M. Klene, J. E. Knox, J. B. Cross, V. Bakken, C. Adamo, J. Jaramillo, R. Gomperts, R. E. Stratmann, O. Yazyev, A. J. Austin, R. Cammi, C. Pomelli, J. W. Ochterski, R. L. Martin, K. Morokuma, V. G. Zakrzewski, G. A. Voth, P. Salvador, J. J. Dannenberg, S. Dapprich, A. D. Daniels, Ö. Farkas, J. B. Foresman, J. V. Ortiz, J. Cioslowski, and D. J. Fox, Gaussian, Inc., Wallingford CT, 2009.

⁹⁸ R. Car and M. Parrinello, *Phys. Rev. Lett.* **1985**, *55*, 2471–2474.

⁹⁹ CPMD v. 3.13.2. copyright IBM Corp., 1990–2009; copyright MPI für Festkörperforschung Stuttgart, 1997–2001. www.cpmd.org.

¹⁰⁰ G.J. Martyna, M.L. Klein and M. Tuckerman, *J. Chem. Phys.* **1992**, *97*, 2635–2643.